AIAA JOURNAL
Vol. 36, No. 7, July 1998

Pressure Oscillations in a Subsonic Cavity at Yaw

P. J. Disimile*
University of Cincinnati, Cincinnati, Ohio 45221-0070
and
N. Toy† and E. Savory‡
University of Surrey, Guildford GU2 5XH, England, United Kingdom

An experimental investigation was undertaken to examine the effect of yaw angle on flow oscillations that occur in an open cavity placed within a subsonic boundary layer. A rectangular cavity with a length-to-depth ratio of unity and a planform aspect ratio of 8.7 was placed within a thick turbulent boundary layer with a corresponding Reynolds number based on the momentum thickness of 10.5×10^3. Pressure time histories were acquired at 15 separate yaw angles using microphone-type pressure transducers. The spectral character of these signals was analyzed, and the pressure levels and dominant frequencies were determined. This study indicates that large changes in the pressure level occur as the yaw angle is changed from 0 to 70 deg. A state of resonance was observed at an angle of 60 deg. Relative sound pressure level calculations indicate that the energy within the cavity increased more than seven times at this orientation. Evidence suggesting a critical angle of approximately 60 deg, as well as mode switching from a fluid dynamic mode to a fluid acoustic mode, is also presented.

Nomenclature

a	= local speed of sound within the freestream, m/s
D	= depth of the cavity, along the transverse direction, mm
$E(f)$	= spectral energy
f	= frequency, Hz
f_D, f_L, f_W	= fundamental acoustic modes based on cavity depth, length, and width, Hz
$f_{e,m}$	= Rossiter's edgetone frequency for mode m, Hz
f_v	= vortex shedding frequency, Hz
f_{x^*}, f_{y^*}, f_{z^*}	= fundamental acoustic modes based on wind-tunnel working section length x^*, width y^*, and height z^*, Hz
H	= boundary-layer shape factor
L	= length of the cavity, dimension along the minor axis when the model is aligned with the streamwise direction, mm
L/D	= length-to-depth ratio of the cavity
M_∞	= freestream Mach number
m	= acoustic mode number used in Rossiter's correlation, $m = 1, 2, 3, \ldots$
Re^*	= unit Reynolds number, m^{-1}
Re_θ	= Reynolds number based on the momentum thickness
Sr_θ	= Strouhal number based on the momentum thickness, $f_v\theta/U_\infty$
U_∞	= freestream velocity, m/s
W	= width of the cavity, dimension along the major axis when the model is aligned with the spanwise direction of the working section, mm
W/L	= planform aspect ratio
X	= streamwise spatial coordinate, mm
Y	= spanwise spatial coordinate, mm
Z	= transverse spatial coordinate, mm
δ	= boundary-layer thickness defined by 99.5% of freestream velocity, mm
δ^*	= boundary-layer displacement thickness, mm
θ	= boundary-layer momentum thickness, mm
ψ	= yaw angle, angle between U_∞ and the cavity minor axis L, deg

Received July 25, 1997; revision received Jan. 23, 1998; accepted for publication Feb. 22, 1998.

*Associate Professor, Department of Aerospace Engineering. Member AIAA.
†Professor and Head of Fluid Mechanics Research Group, Department of Civil Engineering.
‡Fluid Mechanics Lecturer, Department of Civil Engineering.

Introduction

THE presence of a cavity in a surface bounding a fluid flow can cause large pressure, velocity, and density fluctuations in its vicinity, as well as strong propagating acoustic waves. In addition, the drag on the surface can be altered, sensitive instrumentation can be damaged, and structural failure due to resonance can occur. Such flows are of interest in many different areas of engineering. Landing-gear wells, surface-mounted instrumentation on aircraft, and cutouts on marine vehicles are examples of cavities in which the reduction of pressure fluctuations, vibration, noise, and structural fatigue is of great interest.

Cavity flowfields contain a mixture of unsteady flow regimes that may include unstable shear layers that shed vortices in coherent patterns, pressure waves, and resident vortices oriented in the spanwise direction. The shear layer location and generation of self-sustaining oscillations depend on conditions both inside and outside the cavity and, in turn, affect the internal and external flowfields about the cavity. This interaction is the result of an extremely complicated flow pattern that appears to depend on the shape of the cavity (allowing it to be classified as either open, closed, or transitional), Mach number, Reynolds number, and the turbulence characteristics of the approaching boundary layer.[1] Self-sustaining oscillations that are found in cavity flows have been grouped by Rockwell and Naudascher[2] as follows.

1) Oscillations are grouped as fluid dynamic where they arise from the combined effect of shear layer instability amplification and the feedback of downstream disturbances. The presence of large-scale vortical motions in the shear layer is believed to play a major role in this interaction. Standing acoustic waves are not involved in this mechanism, nor is compressibility or high Mach number required.

2) Oscillations are grouped as fluid resonant if the flow oscillations are influenced by and coupled to the standing acoustic waves within the cavity.

3) Oscillations are grouped as fluid elastic when motions of a solid boundary are coupled to the flow oscillations caused by nonlinear interactions between vortex shedding and acoustic wave phenomena.[3]

Both flow-induced and acoustic oscillations due to the presence of rectangular cavities have been studied over the years by many investigators. Rossiter[4] suggested that this phenomenon was a result of acoustic feedback. Vortices that shed periodically from the

upstream lip of the cavity convect downstream and impinge on the aft wall generating an acoustic wave. These acoustic disturbances propagate upstream inside the cavity. Upon reaching the forward lip of the cavity, these waves cause the shear layer to separate and result in the shedding of a new vortex. In this way the vortex and the acoustic disturbances form a feedback loop. Plumblee et al.[5] proposed that the observed tones are a result of cavity resonance and that the frequency of the tones corresponded to the maximum acoustic response of the cavity. In their theory, the turbulent shear layer that spans the cavity opening serves as a broadband noise source that drives the cavity oscillations.

The feedback mechanism described by Block[6] is based on the interaction of the separated shear layer with the boundaries of the cavity. This feedback process begins with the separation of the flow at or near the leading edge of the cavity. As the shear layer impinges on the cavity trailing edge, a disturbance wave is generated and radiated upstream in essentially two distinct paths. One wave (the pressure wave) travels upstream within the cavity; the second wave, generally called the acoustic wave, travels upstream outside the cavity and over the free shear layer. The difference in pressure between the two waves causes the flow at the cavity leading edge to roll up, producing vortices that convect downstream. These new vortices impinge on the cavity trailing edge and again generate sound waves that radiate upstream, thus completing the feedback loop. This feedback loop continuously increases the amplitude of the disturbance waves and is responsible for fluctuating pressure waves and high-intensity tones generated by the cavity.

Tones generated by normal mode resonance were observed for $M < 0.2$, agreeing with Plumbee et al.[5] However, Tam and Block[7] believe that the energy that drives this mechanism is provided by the shear layer instabilities and not the broadband turbulence of the shear layer spanning the cavity. Their measured results indicate that the transition between the normal mode resonance mechanism and the feedback mechanism-generated tones was a gradual process. However, because their model neglected reflections of the acoustic waves at the open end of the cavity, they were unable to account for normal mode resonances. They also assumed a two-dimensional cavity and ignored the mean flow inside the cavity. East[8] suggested the depth mode of not-too-shallow cavities is often excited at very low-subsonic Mach number. This was confirmed experimentally by Tam and Block[7] and by Ahuja and Mendoza.[9]

Although many prior investigations have been conducted to gain insight into the underlying physical behavior of cavity flows,[1,5–8,10–13] only a few works, including that of Rossiter,[4] have made it possible to predict some features of the observed phenomena. Unfortunately, this is limited to situations where the cavity width W spans the flow, i.e., the cavity is oriented at 0-deg yaw. Although limited information is available for yaw angles other than 0 deg (Refs. 14–21), these studies, except for that of Bari and Chambers,[17] examined only a single second yaw angle, either 15 or 45 deg, examined supersonic flow, or reported time mean pressures. Bari and Chambers examined yaw angles from 0 to 30 deg, but their boundary layer was laminar. Therefore, the goal of the present work is to examine the effect of a range of yaw angles on flow oscillations in an open cavity immersed in a turbulent boundary layer.

To accomplish this task an experimental program was undertaken using a single three-dimensional cavity. The present cavity was fabricated with a length-to-depth ratio of unity and placed in a fully turbulent subsonic boundary-layer flow. This model, when oriented along the working section span, i.e., 0 deg, represented an open cavity. A relatively high-aspect-ratio cavity enabled quasi-two-dimensional results to be obtained at 0 deg. The following sections provide details on the cavity model and facility, as well as the results of this experimental program.

Cavity Model

A large rectangular cavity model was constructed using plywood and Masonite®. The dimensions of the cavity were 105 mm in length L, 917 mm in width W, and 105 mm in depth D; see Fig. 1. This provided a relatively wide cavity with a planform aspect ratio W/L of 8.7. Further, this model was configured as an integral part of a turntable that would enable the model to be precisely rotated between 0 and 90 deg in increments of 5 deg (Fig. 2). The turntable

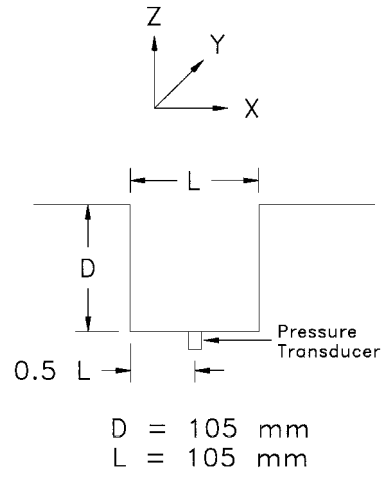

Fig. 1 Schematic of the rectangular cavity.

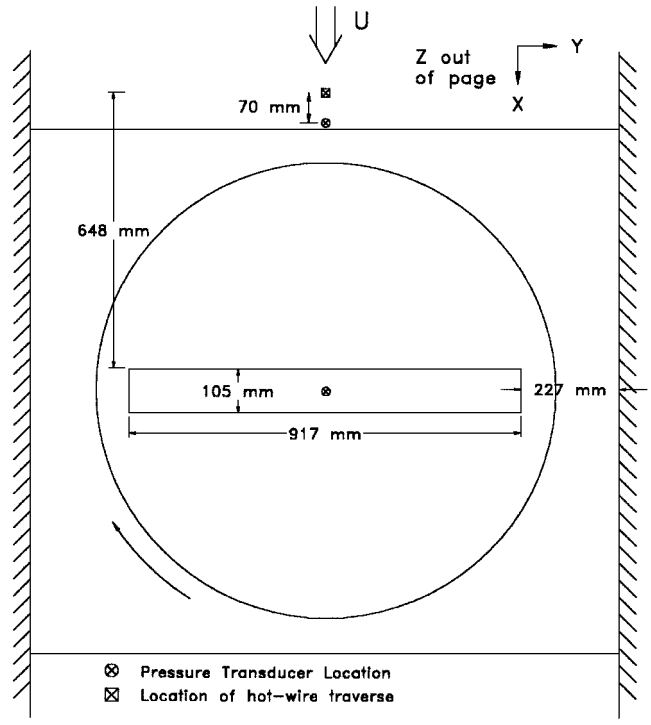

Fig. 2 Working section turntable with cavity model and measurement lacations.

was then placed within the working section of a large, subsonic wind tunnel. An adjustable Masonite insert, capable of providing for different cavity depths, served as the floor of the model. In the present study, this insert was positioned at 105 mm below the surface of the cavity, thereby providing an L/D of 1. This insert also served to hold the cavity floor pressure transducer. A sketch of the cavity designating the location of the cavity pressure transducer is provided in Fig. 1. Figure 2 shows the spatial relationship between the cavity transducer and the upstream boundary-layer transducer, together with the spanwise plane, where the approaching boundary layer was documented.

Experimental Facility

The primary piece of hardware in this research program is the University of Surrey's low-speed, boundary-layer wind tunnel. This is an open-circuit wind tunnel with a centrifugal fan positioned upstream of the working section. The working section of this tunnel has dimensions of 1680 mm in height × 1370 mm in width and extends 9000 mm in length. Because the turntable and cavity protruded above the original test section floor, a temporary false floor was inserted. A shallow ramp of 2.3 deg was inserted at the entrance to the working section, just downstream from the inlet contraction, followed by a false floor. The false floor served as a ground plane

for the cavity model and was fabricated from Masonite, 3.2 mm thick. The Masonite floor was installed with its smooth side facing upward into the flow and extended 7000 mm upstream of the turntable. The addition of this false floor reduced the effective height of the test section by 111 mm. Similarly, the cavity side walls were located 227 mm away from the working section side walls, thereby positioning the cavity major axis perpendicular to the oncoming boundary layer. This orientation is referred to as the zero yaw case, i.e., where the effective streamwise length of the cavity is equal to L of the machined model. The wind tunnel has a maximum speed of 25 m/s and a unit Reynolds number $Re^* = 1.75 \times 10^4$ m^{-1}.

Data Acquisition Strategy

Prior to the acquisition of unsteady pressure data, detailed hot-wire documentation of the approaching boundary layer was performed. This was accomplished by mounting a single 5-μm tungsten hot-wire probe assembly on a computer-controlled traversing mechanism and then performing hot-wire traverses at several locations across the working section of the wind tunnel. As a check for two dimensionality of the approaching flow, five spanwise hot-wire traverses were performed at a location 648 mm upstream from the cavity forward wall. In addition to mean streamwise velocity and turbulence intensity measurements, a separate data set was acquired at a vertical position $Z = 5$ mm above the boundary-layer surface. Specifically, for the case of 0-deg yaw, a time series 20.64 s long was acquired at 16 kHz for the purpose of performing subsequent spectral analysis of the boundary-layer flow close to the wall.

Unsteady pressures were acquired simultaneously at two locations, using surface-mounted pressure transducers. As already stated, one transducer was attached to the cavity floor. This unit was positioned on the centerline, approximately $0.5L$ back from the forward wall of the model and 458 mm away from the model side walls. A second pressure transducer positioned on the streamwise centerline of the tunnel, approximately 685 mm from the working section side walls, was located 578 mm upstream from the boundary-layer separation point, i.e., the forward wall of the cavity. Both pressure transducers used in the present study were an omnidirectional, condenser microphone type. These units have a minimum signal-to-noise ratio of 40 dB and are approximately 10 mm in diameter. Their frequency response was flat within 0.5 dB over the frequency range from 30 Hz to 3 kHz and within 4 dB from approximately 15 Hz to 20 kHz.

Transducer signals were sampled and analyzed using a Hewlett Packard (HP) 3562A dynamic signal analyzer and were resolved over the frequency range from 10 Hz to 10 kHz. The accuracy of the amplitude in the frequency-response measurement mode is specified as ± 0.2 dB. The dynamic range of the signal analyzer is 80 dB, i.e., the difference between the largest and smallest signals that can be measured simultaneously. Although this unit has a maximum frequency response of 256 kHz, the present data were sampled at 25.6 kHz over a period of 8 s. Data being examined in the present study are based on an average of 50 records, with each record consisting of 2048 samples.

The output of the signal analyzer was provided in the form of an energy spectrum $E(f)$. In lieu of separately examining the $E(f)$ of either the cavity transducer or the upstream boundary-layer transducer, it was decided to directly process the unsteady pressure signals within the signal analyzer. Therefore, the effect of ψ on the unsteady pressure within the cavity is presented as a ratio of the $E(f)$ determined from the cavity transducer signal normalized by $E(f)$ of the signal simultaneously supplied by the upstream boundary-layer transducer.

As an analyzer performance check, additional measurements were simultaneously acquired by both the HP analyzer and an external computer-controlled data acquisition system. These data acquisition signals were processed via a commercial fast Fourier transform (FFT) algorithm and compared to the analyzer output. Excellent agreement was noted over the range of values covered by the present study, thereby allowing the analyzer to be used with confidence.

Test Conditions

The wind-tunnel freestream velocity was continually monitored and maintained at 12.16 ± 0.01 m/s for the duration of the experiments. Freestream turbulent intensity measurements indicated a nominal level of 0.28%. Surveys of the wind-tunnel working section indicated that the mean velocity in the test section was uniform to within 2%. Likewise, the streamwise component of turbulent intensity was also determined to be uniform to within 5%. Although the wind tunnel is configured as an open-loop facility that exhausts into a very large laboratory, the temperature in the working section can rise several degrees centigrade over the course of an 8-h test. Therefore, the static temperature in the working section was monitored with a type T thermocouple and was used to correct the freestream velocity. The uncertainties in the static temperature and the hot-wire measurements were estimated to be ± 0.1°C and 1.5%, respectively. The positional accuracy of the hot-wire probe traverses was ± 0.004 mm.

Results

Typical mean velocity and turbulent intensity boundary-layer profiles, acquired above the Masonite floor on the tunnel centerline, are presented in Figs. 3a and 3b, respectively. To enable an accurate assessment of the dimensionality of the approaching boundary layer, five boundary-layer traverses were acquired across the span of the working section. Each traverse was acquired at a streamwise location 700 mm upstream from the forward face of the cavity, at 0-deg yaw. Specifically, spanwise traverses were obtained at the centerline ($Y = 0$) and at ± 200 and ± 400 mm from the centerline. Each boundary-layer profile consisted of hot-wire measurements at 40 spatial locations. The initial position of the hot-wire probe in each traverse was 2 mm above the Masonite floor. To ensure adequate spatial resolution in the Z direction, data were acquired at increments of 2 mm in the range between 2 and 20 mm, at increments of 5 mm when the probe was located between 20 and 100 mm, and at increments of 10 mm for probe positions between 100 and 240 mm.

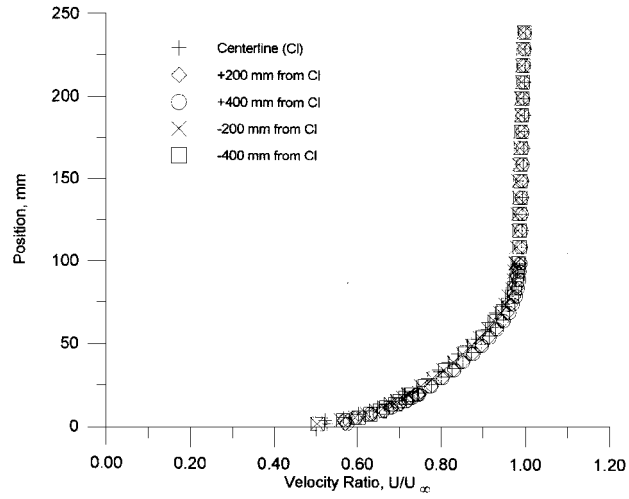

Fig. 3a Upstream boundary-layer mean velocity profile.

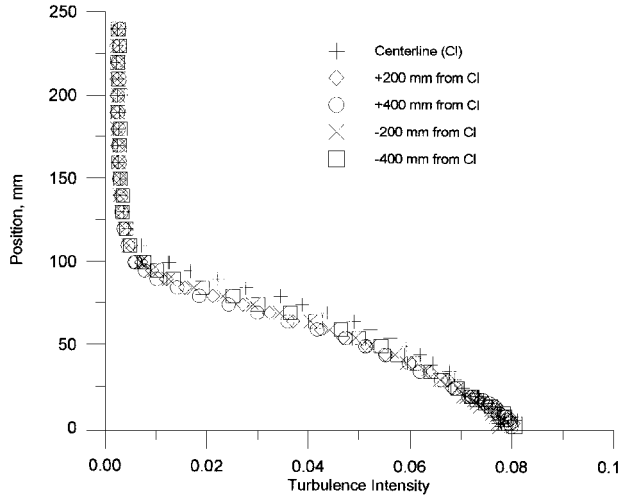

Fig. 3b Upstream boundary-layer turbulent intensity profile.

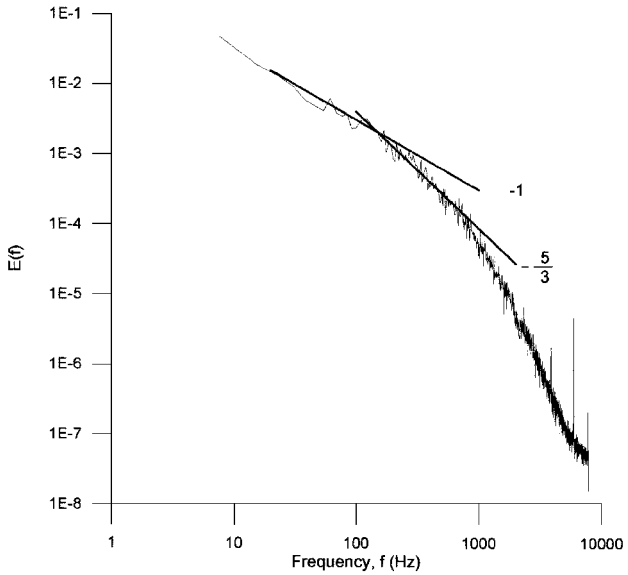

Fig. 4a Energy spectrum of the upstream boundary layer.

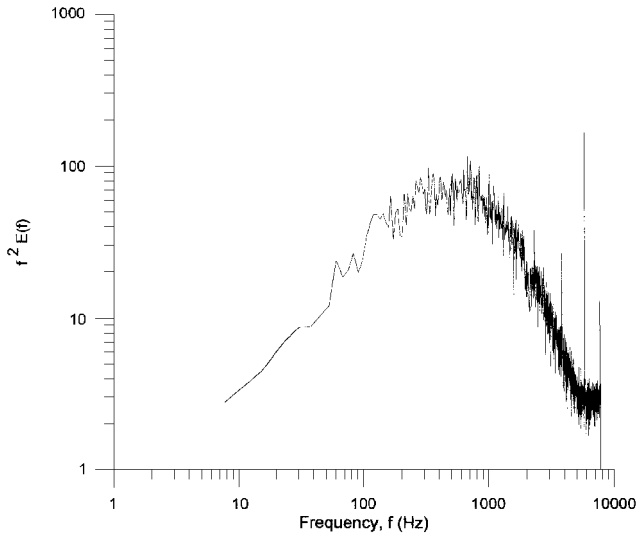

Fig. 4b Dissipation spectrum of the upstream boundary layer.

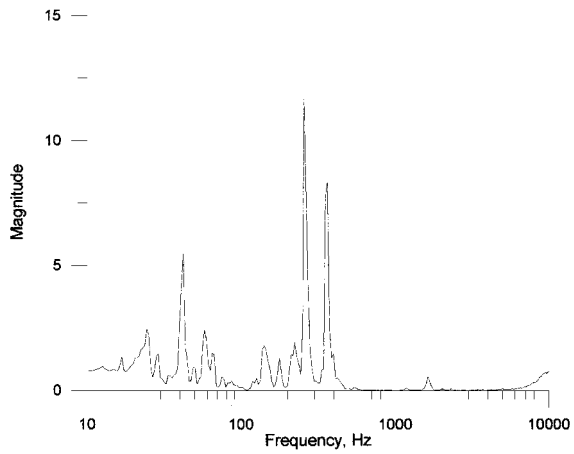

Fig. 5 Normalized boundary-layer energy spectrum with cavity isolated.

Further, documentation of the boundary layer is presented in the spectral data plotted in Figs. 4a and 4b. Figure 4a displays the energy spectrum taken at $Z = 5$ mm above the floor, on the tunnel centerline. Replotting the spectral data, Fig. 4b represents the dissipation spectrum for the same location.

Documentation of the tunnel flow oscillations in the absence of the cavity was achieved by normalizing the boundary-layer transducer signal with that of the cavity transducer in the absence of the

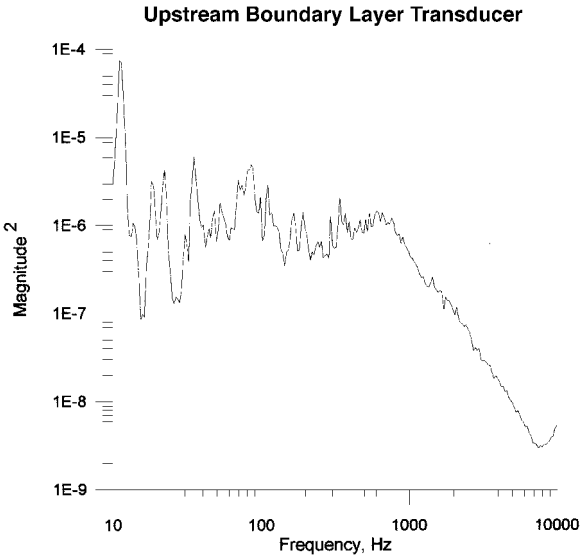

Fig. 6a Typical boundary-layer energy spectrum.

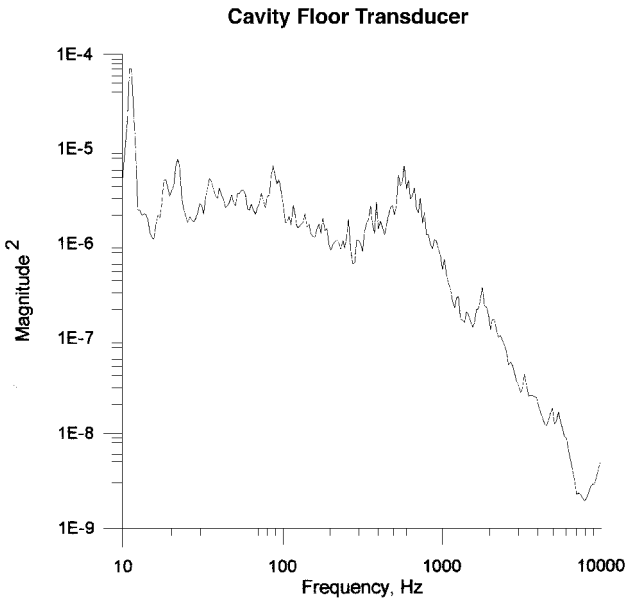

Fig. 6b Typical cavity energy spectrum.

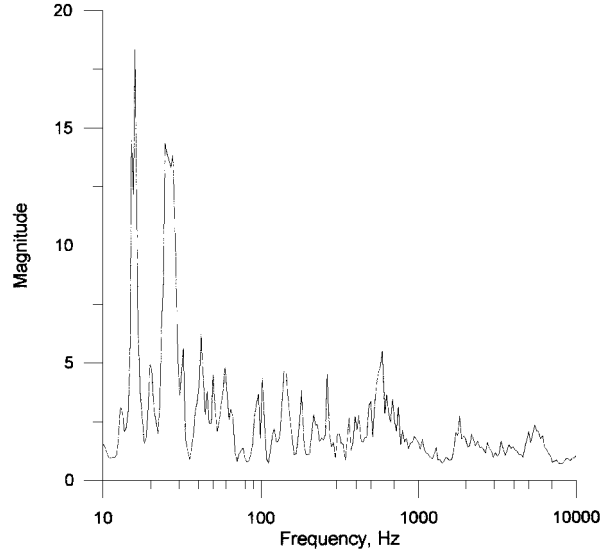

Fig. 6c Typical normalized cavity energy spectrum.

Table 1 Frequency and magnitudes squared of the first three modes

Yaw angle, deg	First mode		Second mode		Third mode	
	Frequency, Hz	Magnitude squared	Frequency, Hz	Magnitude squared	Frequency, Hz	Magnitude squared
0	16	18	25	14	NA	NA
5	16	7	27	6	562	5
10	16	9	26	9	546	6
15	15	10	28	10	546	6
20	14	6	27	5	546	5
25	546	3	43	3	4098	2
30	546	7	16	6	NA	NA
35	546	3	NA	NA	NA	NA
40	24	4	NA	NA	NA	NA
45	15	38	28	32	NA	NA
50	16	105	27	18	NA	NA
55	17	248	NA	NA	NA	NA
60	20	787	16	244	145	158
65	1540	20	NA	NA	NA	NA
70	1372	16	106	14	145	13

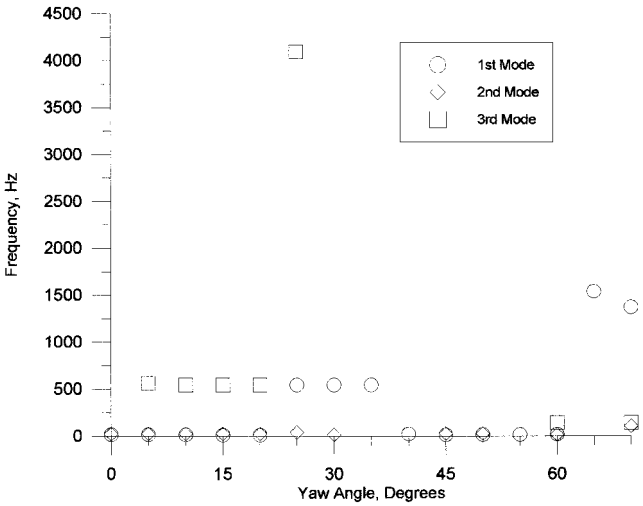

Fig. 7 Frequencies of the first three dominant modes as a function of yaw.

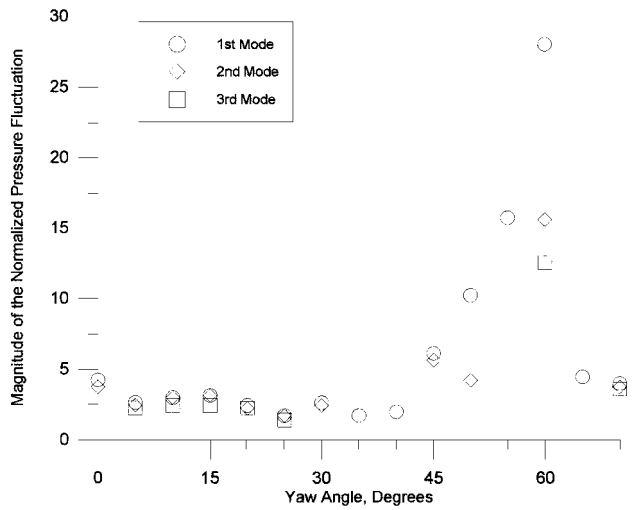

Fig. 8 Magnitude of the normalized pressure fluctuations as a function of yaw.

aerodynamic influences. Specifically, the cavity transducer was energized but isolated from the freestream, thereby allowing the cavity transducer to sense only the background noise and tunnel vibrations. This was accomplished by sealing the cavity opening and isolating the microphone transducer from the freestream. Figure 5 represents a typical normalized boundary-layer energy spectrum in the absence of the driven cavity flow.

A typical cavity and the boundary-layer power spectra with the cavity installed are presented in Figs. 6a and 6b. To enable a quick

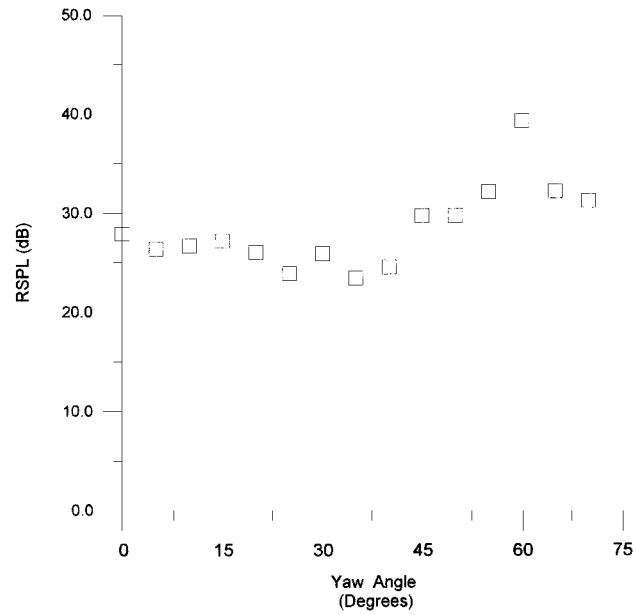

Fig. 9 RSPL as a function of yaw.

assessment of the magnitude and frequency content of the pressure oscillations resulting from the presence of the cavity, without the influence of other tunnel oscillations, the cavity spectra were normalized by energy spectra obtained simultaneously from the boundary-layer transducer (Fig. 6c). The first three dominant peaks of each spectra were identified, and their magnitude squared and frequency are recorded in Table 1. Note that there were several ψ where the second and/or the third dominant modes were not apparent. In this situation, NA appears in Table 1. To examine the effect of cavity yaw, the frequencies of the pressure oscillations for the first three modes vs ψ are presented in Fig. 7. In a similar manner, Fig. 8 displays the magnitude of the normalized pressure fluctuation for the first three dominant modes as a function of ψ. The relative sound pressure level at each angle is presented in Fig. 9.

Discussion

The present experimental study provides an assessment of pressure oscillations resulting from the presence of a rectangle cavity immersed in a thick, subsonic, turbulent boundary layer when subjected to yaw. In such an undertaking one must be concerned with possible wind-tunnel interference that may alter the response of the cavity. Such an interaction can be caused by an acoustic reflection from the opposing tunnel wall, i.e., the ceiling of the working section. Previous work has indicated that this type of interference is unimportant when the ratio of the distance between the opposing surface and the cavity is greater than five.[22] In the present study this ratio is 15.0, and therefore, it is unlikely that the resonant response of

the cavity would be affected by the presence of the wind-tunnel ceiling. Also, the upstream boundary layer was carefully documented and is available as a database for future computational efforts. The following subsections will elaborate on the various aspects of the documentation and the resulting effects of cavity orientation.

Boundary-Layer Documentation

The acquired boundary-layer traverses were analyzed and used to estimate the thickness of the boundary layer δ, the displacement thickness δ^*, the momentum thickness θ, and the boundary-layer shape factor H. Based on the centerline traverse, δ, δ^*, θ, and H were determined to be 210 mm, 18.3 mm, 13.0 mm, and 1.41, respectively. This, in turn, provided for $Re_\theta = 10.5 \times 10^3$. Using the Clauser boundary-layer technique, an estimate of the local skin-friction coefficient and the friction velocity were determined to be 0.0028 and 0.455 m/s. Replotting the velocity data in wall coordinates (u^+ and y^+) and fitting the data with the law of the wall, good agreement was found for an extremely smooth wall.

Comparison of the five hot-wire traverses acquired across the span of the tunnel enabled an assessment of the two dimensionality of the boundary layer within the test domain. Approximately 90% of the cavity width, i.e., 800 mm, was covered by these traverses. The average value of θ was determined to vary by less than 9% across the span of the cavity examined.

Inspection of the energy spectra acquired within the boundary layer 5 mm above the smooth floor documented three distinct regimes of turbulent motions. In the first region, the range of frequencies occupied by the large-scale vortical structures (eddies) is apparent from the line marked by the -1 slope. These motions make the major contribution to the total kinetic energy of the turbulence and are referred to as the energy-containing eddies. In the present study, this region extends up to approximately 100 Hz. Beyond 200 Hz, vortical structures enter into the inertial subrange, as indicated by the tangential line with a $-\frac{5}{3}$ slope (Fig. 4a). Within this region, the effects of viscous dissipation are extremely small compared to the flux of energy transferred by inertial effects. This region begins to fall off at approximately 600 Hz. Finally, beyond this frequency is the dissipation region, where viscous effects dominate. The vortical motions that provide the main contribution to the total dissipation are roughly estimated to be identified by the peak zone evident in the dissipation spectra (Fig. 4b). From Fig. 4b, the maximum dissipation occurs at approximately 690 Hz.

Working Section Flow Oscillations

Prior to examining pressure oscillations resulting from the presence of the cavity, flow oscillations recorded by the upstream boundary-layer transducer in the absence of the cavity are presented in Fig. 5. It is expected that any unsteadiness present in the wind-tunnel working section, including any fan instabilities, would be recorded by this sensor. Inspection of Fig. 5 clearly shows several dominant peaks. The first and most dominant peak is located at 258.5 Hz, with a second peak located at 365.2 Hz. A third peak at 42.2 Hz is also apparent in Fig. 5. To determine the cause of this peak, frequencies of acoustic modes m based on the working section length x^*, width y^*, and height z^* were determined:

$$f_{x^*} = am/2x^*, \qquad f_{y^*} = am/2y^*, \qquad f_{z^*} = am/2z^*$$

Computation of these frequencies produced values of f_{x^*}, f_{y^*}, and f_{z^*} equal to 19.2, 108.1, and 126.3 Hz, respectively. Because the computed value of the first and second modes of f_{z^*} was within 4% of the measured peaks and second mode of f_{x^*} is within 9% of the measured peak, it is assumed that these peaks were related to a harmonic of the fundamental acoustic modes based on the height and length of the wind-tunnel working section.

Frequency of the Cavity Oscillations

Three dominant modes were identified at each of the 15 ψ acquired from 0 to 70 deg. Note that the dominant mode, i.e., the mode representing the largest amplitude, is not necessarily the first peak in the measured FFTs. Typical boundary-layer and cavity spectra at 0 deg are presented in Figs. 6a and 6b, respectively. Inspection of these figures clearly indicates that the largest peak is located at approximately 11 Hz, with nearly equal magnitude in both spectra. Other peaks of interest within the cavity are located at approximately 18, 24, 90, 600, and 1800 Hz. Although minor in nature, the 18- and 24-Hz peaks were also observed when the cavity was covered. However, the nominal 600- and 1800-Hz peaks can be related to cavity acoustic modes. Normalizing the cavity signal by the upstream boundary layer (Fig. 6c), the effects in the cavity are highlighted and the dominant modes at 16 and 24 Hz appear. Although the latter is related to the f_{x^*}, it is believed that 16 Hz is the frequency of vortex shedding from the cavity forward wall.

A subsonic turbulent boundary layer undergoing separation can be related to $Sr_\theta = 0.023$. If the value of θ determined from the hot-wire traverses 648 mm upstream from the separation point is corrected to account for the additional growth between that measurement location and the point where the boundary layer actually separated from the cavity forward wall, then the shedding frequency of the vortices, f_v, can be estimated. This correction provides a value of θ at the cavity separation edge of 13.7 mm. Using the momentum thickness Strouhal number relation, the frequency was then calculated to be 20.4 Hz. Because the dominant frequency recorded in the cavity at 0-deg yaw was 16 Hz, a difference of 21%, a fluid dynamic mechanism related to vortex shedding is suggested. Rockwell and Naudascher[2] note that, when the streamwise cavity length L is much smaller than the acoustic wavelength, the flow oscillations depend on the characteristics of the shear layer and not the acoustic modes of the cavity. Fundamental acoustic modes of the cavity, f_D, f_L, and f_W, were estimated to be 1647 Hz for f_D and f_L and 189 Hz for f_W. This indicates that the acoustic wavelength is approximately twice L, and based on Ref. 2, domination of shear layer characteristics is expected.

A semiempirical approach used to estimate the frequency of cavity pressure oscillations at 0-deg yaw was presented by Rossiter[4] in 1964. Rossiter's correlation [Ref. 4, Eq. (3)] related the frequency of the dominant modes within the cavity produced by vortex shedding to a modified Strouhal number:

$$f_{e,m} = \frac{U_\infty}{L} \frac{m - \gamma}{(1/K + M)}, \qquad m = 1, 2, 3, \ldots$$

where $\gamma = 0.25$ and $K = 0.66$ are constants. Rossiter's Eq. (3) provides the following frequencies for the first three modes: $f_{e,m=1} = 56.03$, $f_{e,m=2} = 130.73$, and $f_{e,m=3} = 205.43$ Hz. However, the dominant cavity frequency recorded in the present study at 0-deg yaw did not match those calculated using this relationship. This is not totally unexpected, inasmuch as Tam and Block[7] showed that Rossiter's[4] model does not work well with other studies, especially when the data are outside the Mach number range covered by his work. In fact, calculations performed by Tam[23] for a two-dimensional rectangular cavity under no-flow conditions indicated that a strong acoustic mode based on cavity depth D should exist. Under the present test conditions, the acoustic frequency of this mode is estimated to be 506 Hz. This value is within 8% of the measured cavity acoustic mode, whose magnitude was significant, but only 35% of the first mode. Tam and Block[7] also showed that, as the Mach number decreased below 0.15, cavity tones appeared to be generated by another mechanism, one supported by Tam's normal mode resonance concept and, therefore, transitioning from vortex shedding to an acoustic mechanism. Because a working section longitudinal acoustic mode already existed at 18 Hz, it is surmised that this mode interacted with the boundary layer to produce strong vortex shedding at 16 Hz. Although this may be considered as a fluid-resonant mechanism, based on previous classifications,[2] it must be emphasized that the acoustic excitation was not supplied by the cavity but by the flow facility.

An inspection of Fig. 7 indicates that the frequency of the dominant oscillation remained constant at nominally 16 Hz up to $\psi = 20$ deg. A similar finding was found by Tracey and Plentovich.[16] In their study they observed no significant difference in the frequency of the pressure signal at 0 and 15 deg. At $\psi = 25$ deg, the frequency of the dominant oscillation jumped to 546 Hz and was observed to remain constant until 35 deg. This jump in frequency coincides with a higher-order harmonic of the fundamental cavity acoustic mode based on width, f_W, thereby indicating a mode switch from fluid dynamic to acoustic.

Beyond this angle, the first mode changed between 15 and 24 Hz, indicative of either a fluid dynamic mode or a wind-tunnel longitudinal acoustic mode. This increase in frequency from 15 Hz at $\psi = 45$ deg to 20 Hz at $\psi = 60$ deg may at first be questioned, but as the model was rotated it became aligned with a thinner boundary layer. Specifically, if one considers the spanwise nonuniformity reported in the boundary-layer documentation section coupled with model rotation into the region of reduced θ, an increase in the frequency of vortex shedding is expected. This provides further support for cavity oscillations based on a fluid dynamic mechanism of vortex shedding. However, at 65 deg the frequency of the measured first mode increased to a maximum of 1540 Hz, which was within 2% of the fundamental cavity acoustic modes based on either f_D or f_L.

In general, a relatively constant second mode at 24 ± 4 Hz was observed, approximately representing the wind tunnel's longitudinal acoustic mode. Except at ψ of 30 and 60 deg, where the second mode was related to vortex shedding, the first mode appears to be either cavity or working section acoustics. In addition, a third mode was observed to reside at the 550 Hz between 5 and 20 deg. Although not apparent at all ψ, this mode appears to be related to the third cavity acoustic mode based on W. However, at 25-deg yaw this mode may have transitioned to a third-order acoustic mode based on either cavity L or D.

Magnitude of the Pressure Oscillations

Plotting the normalized magnitude of the cavity pressure oscillations for all ψ (Fig. 8), the following observations were made. First, the magnitudes of the normalized cavity pressure oscillations represented by the first three dominant modes for all ψ less than 45 deg and greater than 65 deg were found to be between 2.6 and 6.1 times those recorded by the boundary-layer transducer. In addition, the magnitudes of these three modes were essentially equal to one another for ψ less than 30 deg and ψ equal to 70 deg. Second, at ψ between 45 and 65 deg the normalized magnitudes of the pressure oscillations grew an order of magnitude.

At $\psi = 60$ deg a state of resonance was observed, where the normalized magnitude of the cavity oscillations grew to the greatest levels. The most dominant oscillation, i.e., the first mode, reached a level approximately 28 times larger than that recorded by the upstream transducer. Similarly, peaks in the second and third modes grew to levels 15 and 12 times larger than those recorded by the boundary-layer transducer.

Relative Sound Pressure Levels

Typically, time histories of the surface pressures are used to calculate sound pressure levels (SPL) within the cavity using the following equation:

$$\overline{\mathrm{SPL}} = 10 \log_{10} \frac{(\bar{\dot{p}}^2)_{\mathrm{cavity}}}{20 \times 10^{-6}} \tag{1}$$

where 20×10^{-6} Pa is a standard reference value used in acoustics and

$$\bar{\dot{p}}^2 = \frac{1}{F} \int_{f_1}^{f_2} (p - \bar{p})^2 \, \mathrm{d}f \tag{2}$$

However, to determine the effect of yaw on changes in the cavity environment related to the upstream conditions, i.e., the boundary layer, a relative SPL (RSPL) was calculated as follows:

$$\overline{\mathrm{RSPL}} = 10 \log_{10} \left[\frac{(\dot{p}^2)_{\mathrm{cav}}}{(\dot{p}^2)_{\mathrm{bl}}} \right] \tag{3}$$

Therefore, the values calculated using Eq. (3) provide direct information on the relative change in SPL resulting from the addition of the cavity, as well as any SPL change due to ψ. Using a sound-level meter, a baseline sound level (decibels) in the absence of the cavity was recorded. Under the present test conditions, this value was determined to be approximately 75.5 dB.

Calculation of the RSPL enabled one to determine whether a particular mode was amplified at the expense of another or whether the total energy contained within the cavity as represented by the RSPL increased (Fig. 9). Although a particular mode may have been enhanced, inspection of Fig. 9 clearly shows that the RSPL drops by approximately 3 dB up to $\psi = 40$ deg. Beyond this angle, the RSPL increases, peaking at 39.3 dB, indicating more than an 11-dB increase over the $\psi = 0$ deg orientation. This can be equated to an energy increase of approximately 12.6 times. As one continues to inspect Fig. 9 for angles greater than 60 deg, a dramatic decrease in RSPL is noted. All in all, the 60-deg model orientation appears to excite cavity unsteadiness into a state of resonance. As is apparent in Fig. 8, this addition of energy produces pressure oscillations more than 28 times that present in the upstream boundary layer. Nevertheless, the mechanism responsible for this resonance appears to be quite complex, having definite acoustic components, some of which have been coupled to the shedding of the vortices within the shear layer.

Although previous researchers have felt that the shear layer spanning the cavity provided the energy responsible for cavity oscillations, the source of this energy is disputed. Plumbee el al.[5] suggested the energy was a result of broadband turbulence. Tam and Block[7] believed the shear layer instabilities were the source. An inspection of Fig. 4b, the boundary-layer dissipation spectra, shows the region of maximum dissipation to occur between 650 and 850 Hz. Within this region, energy is directly dissipated by viscous forces. It is highly unlikely that sufficient quantities of energy are available to excite the cavity in the 10–20 Hz range. Therefore, the present study offers no support for the Plumbee et al.[5] model. The Tam and Block[7] hypothesis of shear layer instability as the mechanism for energy transfer to the cavity appears to be more probable, in view of the availability of boundary-layer energy in the low-frequency range (Fig. 4a). Large vortical motions that occupy the low-frequency range of the spectra (less than 100 Hz) contain energy levels two orders of magnitude higher than vortices in the dissipation region. Therefore, it is more likely that some of this energy would be available for coupling to cavity oscillations. However, because of the inherent acoustic modes present in the flow facility, it is believed that the facility is the source of excitation that is responsible for an added degree of organization in the large-scale motions, within the shear layer, thereby producing an efficient coupling between the shear layer instabilities and cavity oscillations.

In trying to understand the significance of a critical ψ, the results reported in previous studies are also reviewed. In a previous low-speed experiment by Savory et al.[18] using cavities with a planform ratio of 2 and varying depths, it was shown that the largest time mean drag force was experienced by the cavity at approximately $\psi = 60$ deg. SPL reported by Disimile and Orkwis[20,21] at supersonic speeds indicate that a local SPL maximum, approximately 3 dB above the background level, occurred at approximately 57.5-deg yaw. Finally, early subsonic studies of triangular cavities by Torda and Patel[24] found cavities with an equivalent $\psi = 60$ deg, i.e., cavities with a 60-deg apex angle, between the oncoming flow and the leading edge, were observed to undergo a state of resonance. However, when the apex angle of the cavity was changed to 30 deg, i.e., an equivalent $\psi = 75$ deg, resonance would not occur. Results of the present study, supported by previous research, suggest that in addition to the present listing of critical parameters, the orientation of the leading edge must be included when considering the cavity resonance. In addition, the research appears to suggest a critical orientation for the leading edge of a cavity. This critical angle, approximately 60 deg, seems to be insensitive to speed and compressibility effects.

Conclusion

This study examined the effect of model orientation on the unsteady pressure within the cavity. Using a rectangular cavity with an L/D of unity and a planform aspect ratio of 8.7, the magnitude and frequency of cavity pressure oscillations were recorded. These results show that the cavity undergoes mode switching from a fluid dynamic state to a fluid acoustic state depending on the efficiency of the coupling between the working section acoustic modes and the cavity acoustic modes. A state of fluid acoustic resonance was observed to occur at $\psi = 60$ deg, which may in part be related to the orientation of the cavity leading edge, i.e., the cavity forward wall. Under these conditions, energy within the cavity was found to increase an order of magnitude, producing pressure oscillations

28 times higher than that recorded by the upstream boundary-layer transducer.

Acknowledgments

The authors wish to thank the University of Cincinnati for providing P. J. Disimile with academic leave in England and the University of Surrey for providing wind-tunnel time and technical support. In addition, the authors greatly appreciate the engineering support of Curtis W. Fox.

References

[1]Rockwell, D., and Naudascher, E., "Self-Sustained Oscillations of Impinging Free Shear Layer," *Annual Review of Fluid Mechanics*, Vol. 11, 1979, pp. 67–94.

[2]Rockwell, D., and Naudascher, E., "Review: Self-Sustaining Oscillations of Flow Past Cavities," *Transactions of the American Society of Mechanical Engineers*, Vol. 100, June 1978, pp. 152–165.

[3]Issacson, L. K., and Marshall, A. G., "Nonlinear Interactions in Internal Cavity Flows," *AIAA Journal*, Vol. 21, No. 5, 1983, pp. 785, 786.

[4]Rossiter, I. E., "Wind Tunnel Experiments on the Flow Field over Rectangular Cavities at Subsonic and Transonic Speeds," Aeronautical Research Council, R&M No. 3438, London, Oct. 1964.

[5]Plumblee, H. E., Gibson, J. S., and Lassiter, L. W., "A Theoretical and Experimental Investigation of the Acoustic Response of Cavities in Aerodynamic Flow," WADD, TR-61-75, Wright–Patterson AFB, Dayton, OH, 1962.

[6]Block, P. J. W., "Noise Response of Cavities of Varying Dimensions at Subsonic Speeds," NASA TN-D-8351, Dec. 1976.

[7]Tam, C. K. W., and Block, P. J. W., "On the Tones and Pressure Oscillations Induced by Flow over Rectangular Cavities," *Journal of Fluid Mechanics*, Vol. 89, Pt. 2, 1978, pp. 373–399.

[8]East, L. F., "Aerodynamically Induced Resonance in Rectangular Cavities," *Journal of Sound and Vibration*, Vol. 3, No. 3, 1966, pp. 277–287.

[9]Ahuja, K. K., and Medoza, J., "Effects of Cavity Dimensions, Boundary Layer, and Temperature on Cavity Noise with Emphasis on Benchmark Data to Validate Computational Aeroacoustic Codes," NASA CR-4653, April 1995.

[10]Karamcheti, K., "Acoustic Radiation from Two-Dimensional Rectangular Cutouts in Aerodynamic Surfaces," NACA TN-3487, Aug. 1955.

[11]Tam, C. J., Orkwis, P. D., and Disimile, P. J., "A Comparison of Baldwin–Lomax Turbulence Models for Two-Dimensional Open Cavity Computations," *AIAA Journal*, Vol. 34, No. 3, 1996, pp. 629–631.

[12]Tam, C. J., Orkwis, P. D., and Disimile, P. J., "Algebraic Turbulence Model Simulations of Supersonic Open Cavity Flow Physics," *AIAA Journal*, Vol. 34, No. 11, 1996, pp. 2255–2260.

[13]Tam, C. J., Orkwis, P. D., and Disimile, P. J., "Variations in Flow Field Physics Caused by Algebraic Turbulence Model Modifications for a Supersonic Two-Dimensional Open Cavity," AIAA Paper 97-0660, Jan. 1997.

[14]Plentovich, E. B., Chu, J., and Tracy, M. B., "Effect of Yaw Angle and Reynolds Number on Rectangular-Box Cavities at Subsonic and Transonic Speeds," NASA TP-3099, July 1991.

[15]Tracy, M. B., Plentovich, E. B., and Chu, J., "Measurements of Fluctuating Pressure in a Rectangular Cavity in Transonic Flow at High Reynolds Numbers," NASA TM-4363, June 1992.

[16]Tracy, M. B., and Plentovich, E. B., "Characterization of Cavity Flow Fields Using Pressure Data Obtained in the Langley 0.3-Meter Transonic Cryogenic Tunnel," NASA TM-4436, March 1993.

[17]Bari, A., and Chambers, F. W., "Shear Layer Resonance over Open Cavities at Angles to the Flow Direction," AIAA Paper 93-4397, Oct. 1993.

[18]Savory, E., Toy, E., Disimile, P. J., and DiMicco, R. G., "The Drag of Three-Dimensional Rectangular Cavities," *Journal of Applied Scientific Research*, Vol. 50, 1993, pp. 325–346.

[19]Disimile, P. J., DiMicco, R. G., Lueders, K., Savory, E., and Toy, N., "Unsteady Flow in a Three-Dimensional Rectangular Cavity Immersed in a Subsonic Crossflow," *ASME Conference, Forum on Unsteady Flow* (Atlanta, GA), Vol. 102, American Society of Mechanical Engineers, New York, 1990, pp. 45–50.

[20]Disimile, P. J., and Orkwis, P. D., "Effect of Yaw on Pressure Oscillation Frequency Within Rectangular Cavity at Mach 2," *AIAA Journal*, Vol. 35, No. 7, 1997, pp. 1233–1235.

[21]Disimile, P. J., and Orkwis, P. D., "Sound-Pressure-Level Variations in a Supersonic Rectangular Cavity at Yaw," *Journal of Propulsion and Power*, Vol. 14, No. 3, 1998, pp. 392–398.

[22]McGregor, O. W., and White, R. A., "Drag of Rectangular Cavities in Supersonic and Transonic Flow Including the Effects of Cavity Resonance," *AIAA Journal*, Vol. 8, No. 11, 1970, pp. 1959–1964.

[23]Tam, C. K. W., "The Acoustic Modes of a Two-Dimensional Rectangular Cavity," *Journal of Sound and Vibration*, Vol. 49, 1976, pp. 353–364.

[24]Torda, T. P., and Patel, B. R., "Investigations of Flow in Triangular Cavities," *AIAA Journal*, Vol. 7, No. 12, 1969, pp. 2365, 2366.

S. Glegg
Associate Editor